PROCEEDINGS, 45th Workshop on Geothermal Reservoir Engineering
Stanford University, Stanford, California, February 10-12, 2020
SGP-TR-216

# Analyzing Fracture Flow Channel Area in EGS Collab Experiment 1 Testbed

Pengcheng Fu, Hui Wu, Xin Ju, and Joseph Morris

Atmospheric, Earth, and Energy Division, Lawrence Livermore National Laboratory, Livermore, CA 94550

fu4@llnl.gov

**Keywords:** EGS Collab, fluid circulation, leakoff, hydraulic fracture

## ABSTRACT

The EGS Collab Experiment has stimulated a fracture network in the 10 m-scale to study stimulation and fluid circulation processes related to engineered geothermal systems. While microseismic survey resolved the overall dimensions of the main hydraulic fracture in the fracture network, the extent to which flow during the long-term circulation test is channelized remains poorly constrained. In this paper, we reason that a consistent observation in several short-term injection tests, which took place in early 2019, provides information to infer the total width of flow channels. By mapping the problem to a leakoff-dominated fracturing model, we estimate the total flow channel width to be 3 m. A thermal modeling effort utilizing this result found that only a fraction of a 1°C of temperature drop is expected after nearly one year of circulation. This small temperature signal has likely been obscured by the Joule-Thomson effect, which is expected to increase the fluid temperature by several degrees at where the temperature is measured.

## 1. INTRODUCTION

The EGS (enhanced geothermal system) Collab project, sponsored by the United States Department of Energy (DOE), Geothermal Technologies Office (GTO), focuses on intermediate-scale (~10-20 m) EGS reservoir creation processes and related model validation in hard, low-permeability rocks [Kneafsey et al., 2020]. The first phase (referred to as "Collab Experiment 1" or "Experiment 1") of the project has been underway at the West Access Drift of the Sanford Underground Research Facility (SURF) in South Dakota at 4850 ft (1478 m) below ground since early 2018. Through multiple hydraulic stimulations, we have created a fracture network comprised of both hydraulic fractures (created in the tensile mode) and natural fractures (pre-existing). A long-term circulation test started in late March 2019 and has continued largely continuously since then, recently sustaining a fluid recovery ratio higher than 95%.

The fracture system engaged in the long-term circulation test has been delineated with strong evidence from multiple types of field data, including detailed wellbore logs, highly accurate microseismic (MEQ) imaging, distributed temperature sensing from observation wells, and direct observation of fracture intersections with an open-hole wellbore [Fu et al., 2019]. MEQ imaging allowed an estimation of the extents of the hydraulic fracture as detailed in the next section. However, it is well known that flow channeling is ubiquitous in fracture networks [Tsang and Tsang, 1989; Guo et al., 2016]. In other words, a fraction, often a relatively small fraction, of the total fracture surface area carries the majority of the flow, forming flow channels. The severity of flow channeling, quantifiable by the total area of the flow channels, has import implications for the performance of EGS, as it is this flow-carrying area instead of the total fracture area that determines the heat production performance. For the Collab Experiment 1 testbed, quantifying the fracture flow channel area is also important for interpreting experiment data, particularly the conservative tracer data [Neupane et al., 2020]. Such tracer data provide indications of the "fracture volume" (area x aperture) engaged in the flow field. Combing this fracture volume and the flow channel area would allow an estimation of the fracture aperture.

Quantifying such flow-carrying area is intrinsically difficult. As mentioned above, conservative tracer tests provide some indication of the fracture volume, but not fracture area. Adsorbing tracer tests can provide useful information of fracture surface area swept (Hawkins et al., 2018). However, the excessively or insufficiently adsorption of an adsorbing tracer will inevitably cause inaccuracy in the estimate of the fracture area. Geophysical methods, such as MEQ imaging, electrical resistivity tomography (ERT), and active seismic methods such as CASSM, could have the necessary resolution for resolving the overall dimension of a fracture if the accuracy and spatial coverage of the sensors are optimal, such as in the highly instrumented Collab Experiment 1 testbed. However, the "geophysically differentiable fracture area", that is, the area that produces certain geophysical signals or signatures, is only loosely related to the flow-carrying aspect of a fracture.

We present an innovative method to infer the total flow channel area of a fracture or fracture network by considering unique behavior of fluid flow in an opening-mode fracture. The main experiment data that this method relies on is the arrival time of fluid at the production well. In this paper, we first review the evidence used to constrain the overall configuration of the fracture system engaged in the flow test. We then describe the rationale and equation for fluid front propagation in a fracture in the leakoff-dominated regime. Finally, we use the estimated flow channel area to predict the thermal response of the testbed if the circulation test were to continue for a longer duration.

## 2. THE FRACTURE FLOW NETWORK

Thanks to the extensive site characterization work and the multiple means of monitoring, the flow network resulting from the hydraulic stimulations and engaged in the flow test can be delineated with great confidence.

### 2.1 OT-P Connector, a Prominent Natural Fracture

According to well logs and core logs, five out of the eight wells at the testbed intersect a prominent natural fracture with variable yet overall large aperture, as shown in Figure 1. In a low-pressure hydraulic testing soon after drilling the wellbores and before any stimulation, it was found that this fracture establishes a strong hydraulic connection between well E1-OT and E1-P, through which fluid can flow under a very low pressure difference. We hence call this fracture the "OT-P Connector". Microseismic events observed during the multiple stimulations from May 22 to June 25, 2018 indicated that the OT-P Connector causes remarkable discontinuity in the propagation trajectories of the hydraulic fracture.

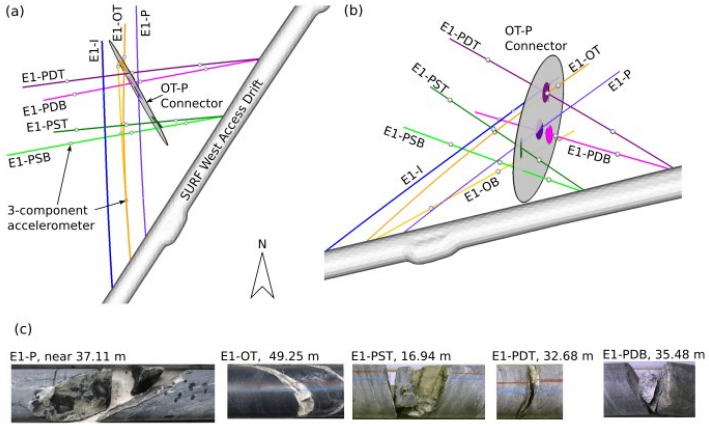


**Figure 1 Delineating OT-P Connector, a prominent natural fracture in the testbed. The locations and orientations of the intersection traces with each well are shown as small disks. (a) and (b) shows the wellbores and the fitted OT-P Connector plane from two angles. (c) shows images of cores where this natural fracture's intersections with five wells.**

### 2.2 The Main Hydraulic Fracture(s)

The long-term circulation test is injecting fluid into an open-hole section centered at 50 m (164 ft) depth in well E1-I. The hydraulic stimulations targeting this section occurred on May 22, 23, 24, 25, and June 25, over multiple stimulation "episodes". Driven by a strong thermal stress gradient rooted in the cooling surrounding the mine drift during the many decades of mining operations, the hydraulic fracture propagated eastward toward OT-P Connector and the drift, as predicted by modeling results [Fu et al., 2018]. Between the injection point and OT-P Connector, the microseismic events conform to a largely vertical plane that is approximately perpendicular to the minimum principal stress direction estimated based on prior tests (Oldenburg et al., 2016). The microseismic cloud did eventually propagate to the east of OT-P Connector during a longer stimulation episode on May 25 (the second episode on that day) and also during a stimulation of the same interval on June 25. Two distinct planar features east of OT-P Connector were created/stimulated by these injections, and they significantly deviated from the planar feature west of OT-P Connector. During a hydraulic stimulation from the nominal "production well" E1-P on June 25, microseismic events only appeared east of OT-P Connectors, strengthening the two eastern planar features.

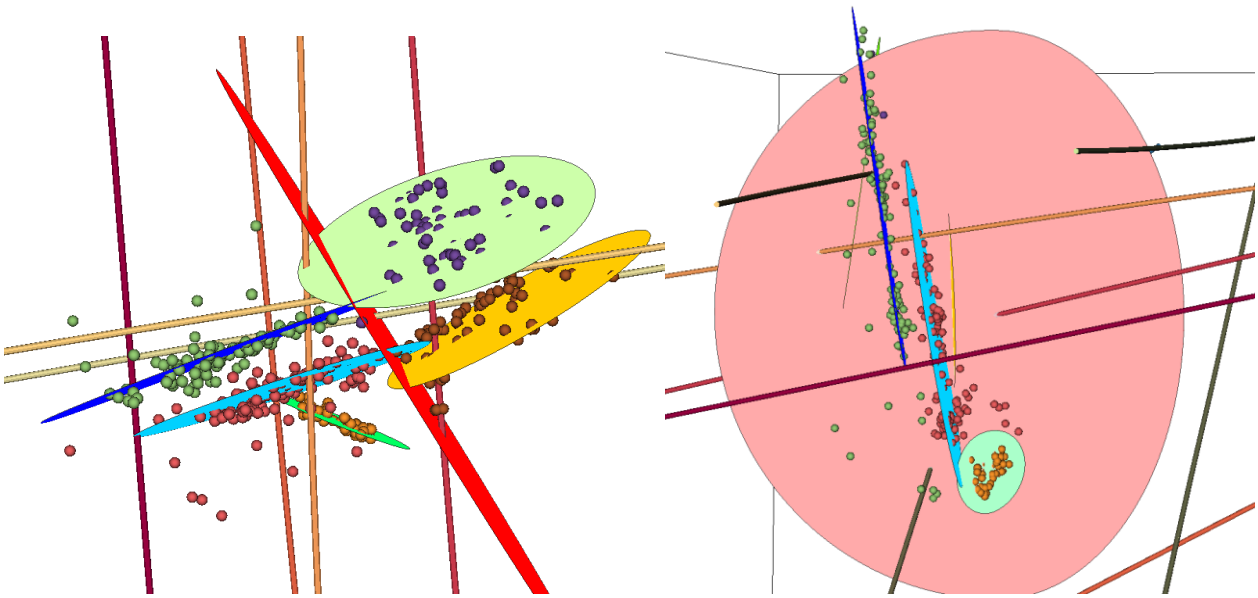

**Figure 2 Microseismic events and fitted fracture planes.**

A close inspection of the main microseismic cloud between well E1-I and OT-P Connector reveals that it is comprised of two parallel planes, both largely vertical and trending east-west. The northern plane, denoted "HF-north", strikes 72.0° and dips 81.9, whereas its southern counterpart, "HF-south", strike 75.5° and dips 79.0°. While these two planes significantly overlap, HF-north seems to occupy the higher part of the testbed space while HF-south mostly propagated downwards. There is a smaller planar feature, striking 113.5° and dipping 86.5°, growing toward southeast from the bottom of HF-south. This feature is believed to be caused by a natural fracture. Since it is small and does not provide hydraulic connection between any other features (fractures and wellbores), its role is not considered in our analysis.

The presence of two parallel hydraulic fractures between well E1-I and OT-P Connector is corroborated by observations on DTS data. As shown in Figure 3., the May 23 stimulation only caused a temperature anomaly in well E1-OT at 47 m deep. The May 24 stimulation intersected E1-OT at both 45.5 m and 47 m deep. In the two stimulations on May 25, the temperature anomaly at 47 m deep became dominant. In the current analysis, we conceptually treat the two hydraulic fracture planes as one plane as the two closely spaced parallel planes have litter overlap in the vertical direction. In regard to fluid leakoff from fracture into rock matrix, such a simplification is reasonable.

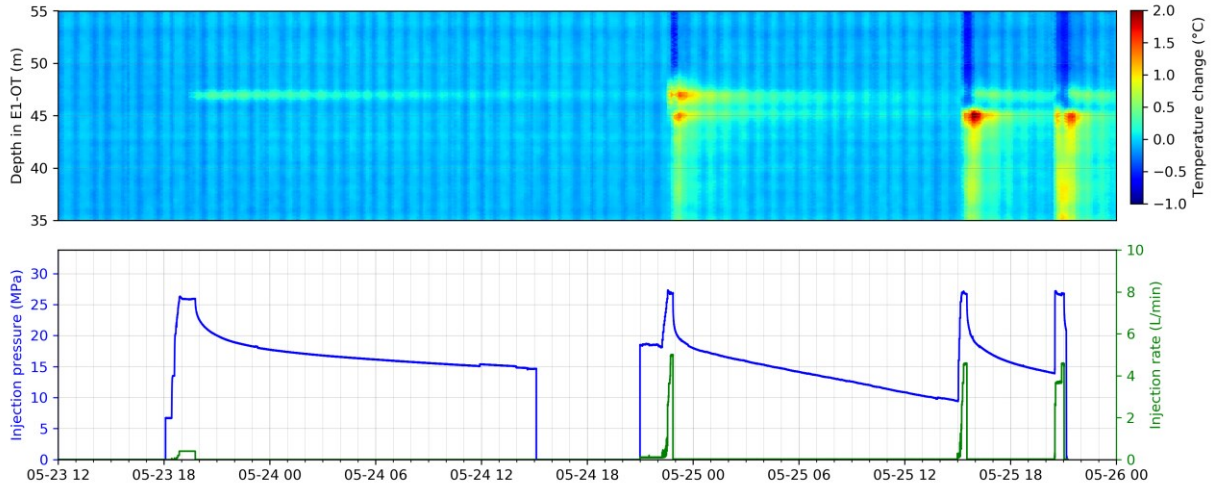


**Figure 3 DTS measurement of temperature change from the baseline temperature along well E1-OT during the hydraulic stimulations between May 23 and May 25.,**

### 2.3 The Flow Network Model

The simplified flow network consisting of two wellbores and two fractures, an effective hydraulic fracture and the OT-P Connector, is shown in Figure 4. As reasoned above, the hydraulic fracture represents the effects of the two closely spaced but minimally overlapped hydraulic fracture planes. The hydraulic fracture directly intersects well E1-P at approximately 127 ft to 129 deep. Part of the injected fluid is recovered from this intersection. The hydraulic fracture also intersects OT-P Connector, and OT-P Connector in turn intersects well E1-P at approximately 121 ft deep. Part of the injected fluid is fed into OT-P Connector through the intersection between these two fractures, and part or all of that fluid is recovered from the intersection between OT-P Connector and well E1-P. In well E1-P, two packers straddle across the intersection with OT-P Connector at 121 ft deep. The flowmeter that measures the outflow rate from this natural fracture is denoted channel "PI" because the flow is from the packer "interval". The intersection(s) with the hydraulic fracture(s) is below the lower packer, and that channel is termed "PB", with B stands for "bottom".

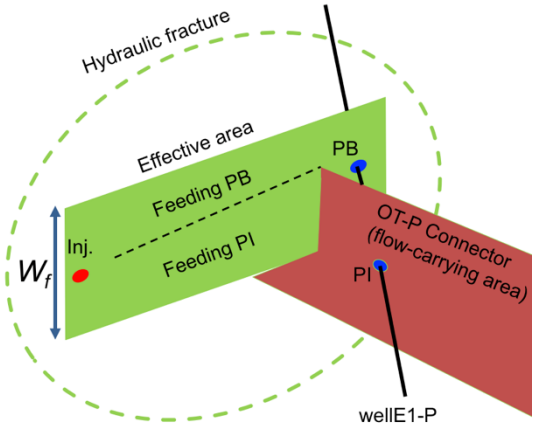


**Figure 4 Conceptual flow network model for the current analysis.**

Only the hydraulic fracture area west of OT-P Connector is included in the simplified model. In more recent flow data, as the system is more saturated, more than 90% of the injected fluid is recovered from the two fracture intersections along E1-P. This indicates that little fluid reaches east of OT-P Connector and the hydraulic fractures to the east are like "dead ends" for flow.

Microseismic data suggest that the overall height of the hydraulic fracture(s) is as large as 20 m. In Figure 4, we show that the "flow-carrying" part of the hydraulic fracture, conceptualized as a rectangle with a width of $W_f$ and spanning between the injection and production wells, is a fraction of the total height of the hydraulic fracture. The width of the idealized fracture, $W_f$, represents the total width of the flow channels.

Although for this testbed we have an unusual amount of data and information to infer the flow network as described above, there is still a great deal of uncertainty in the detailed flow distribution. For example, the total fluid recovery ratio has been largely stable with a slow yet steady increasing trend, but the allocations among various outlets, particularly between PI and PB have fluctuated over time, implying evolving flow fields or at least dynamic flow allocation at the interface between the hydraulic fracture and OT-P Connector. Despite the dynamic and uncertain nature of the flow network, an important fact that enables the subsequent analysis is that the diversion of injected fluid from the main hydraulic fracture occurs near the main outlet of fluid, namely the intersection with well E1-P.

The main objective of this study is to infer $W_f$, which is the total width of flow channels between the injection well and the production well and between the injection well and the connection with OT-P Connector.

## 3. KEY FIELD OBSERVATIONS

### 3.1 A Brief History of the Testbed

The testbed has been subjected to multiple stimulation treatments and hydraulic circulation tests. Apart from the stimulations centered around the mechanical notch at 164 ft deep as described in section 2.1, stimulations were also performed at 142 ft and 128 ft deep in well E1-I. The responses from these three locations were quite different but there was no sign of hydraulic communication among the fractures stimulated from these three intervals. Therefore, there is no need to present specific details about the stimulations at 142 and 128 ft deep.

Between late October and late November 2018, a suite of circulation tests were performed by injecting into the 164 ft interval of E1-I. Experiments included constant rate (mostly 400 ml/min) injection, high rate stimulation when injection pressure increased at an unacceptable rate, altering the water source and chemical compositions, and cooling the injected fluid. The tests were plagued by unexpected issues most likely caused by geochemical and/or biological processes. The uncontrollable injection pressure increase forced the tests to terminate and the team to seek additional stimulations from the 142 ft internal in December 2018.

When the 142 ft interval stimulations did not yield a viable flow path, owing to a natural fracture set blocking the flow path between the injection and production wells and damage to observation wells, the focus of the experiment returned to the 164 ft interval.

### 3.2 Key Observations for the Current Study

Between February 4 and 7, 2019, various injection configurations were experimented included short-term pressurization of E1-P, the nominal production well. Starting on February 20, the focus was shifted to evaluating whether reproduceable responses to 400 ml/min injection at the 164 ft interval could be attained from the testbed. The experiment consisted of multiple injection tests, all at a nominal rate of 400 ml/min. These tests each lasted between four hours and two days, with variable idling periods between them as shown in Figure 5. The long-term injection started on March 27, 2019 and has continued except for several relatively minor interruptions (mostly due to equipment issues) into February 2020 and is still underway.

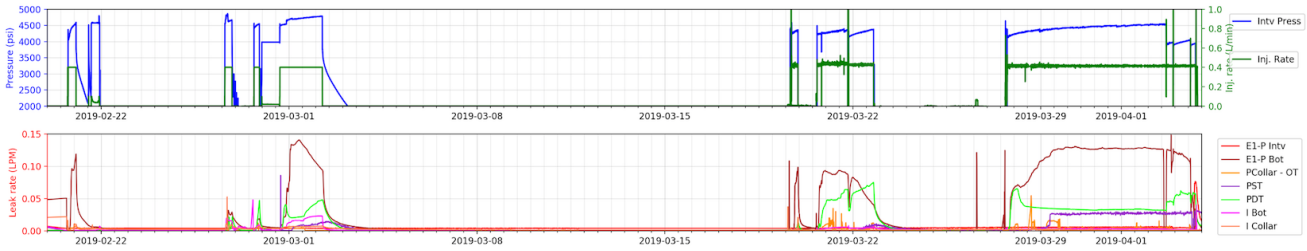


**Figure 5 Injection and fluid recovery in a series tests between late February and early April, 2019. The upper panel shows the injection pressure (blue) and injection rate (green). The lower panel shows the fluid recovery rates from several channels. Because the part of the purpose was to test the system, some repurposing of the recovery rate channels took place in this time window.**

The key observation used in the current study is that it took approximately two hours from the start of injection for water to flow out of the intersection between the hydraulic fracture and well E1-P (i.e. flow channel PB). We only consider the injection tests each with at least 4 days of inactivity in the testbed prior to the test to ensure that the effects of prior injection have dissipated. These include the injections that started on Feb. 21, Feb. 26, Mar. 19, and Mar. 27, 2019. The results of these four tests are shown in Figure 6. They had the same injection rate, 400 ml/min; and they also had similar, and largely constant over time, injection pressure, reflecting the "pressure-limiting" behavior, typical of flow through an open fracture. In all cases, fluid arrived at E1-P after approximately 2 hours of injection. Note that for these four tests, the lower packer in E1-P was not inflated so that the PI and PB intervals were not separated. Based on results in April 2019, when the lower packer was inflated, fluid was expected to arrive at PB much earlier than at PI. Therefore, the arrival time was controlled by fluid arriving at well E1-I through the hydraulic fracture, although the later measurements likely included contributions from both PI and PB. The consistency among the fluid arrival time at E1-I was especially remarkable as we notice how variable the actual flow rate though E1-P was and how variable the arrival time at well E1-PDT was.

## 4. ESTIMATING THE FLOW CHANNEL AREA

### 4.1 Leakoff rate estimation

Based on the consistency in the data, it is reasonable to hypothesize that the fluid arrival time at E1-P reflects how fluid front caused by the injection propagates along the hydraulic fracture in the "leakoff-dominated" propagation regime. To verify that it is indeed in the leakoff-dominated regime, we calculate the expected leakoff rate.

The Carter's leakoff coefficient which is usually used as an empirical coefficient, can be related to physical properties of the rock by assuming 1D diffusion.

$$C_L = \Delta P \left(\frac{k\phi C_t}{\pi\mu}\right)^{0.5}$$

The following list explains the parameters and justifies the values used in this work.

- $\Delta P$ is the pressure difference driving the diffusion. Assuming an open fracture and ignoring frictional loss (which is small for an open fracture), it is the injection pressure minus the *in situ* pore pressure. Owing to the long drainage history around the mine drift, we assume the pore pressure is approximately atmospheric pressure. Therefore, we choose $\Delta P$=4350 psi or 30 MPa.
- $k$ is the intrinsic permeability of the rock. The host rock is high heterogeneous and has foliation planes and natural fractures. According to Frash et al. (2019), intact Poorman schist has permeability no greater than 1 μD while intact foliation has permeability as high as tens of mD. We tentatively use $k$ = 2 μD in the current work.
- $\phi$ is the rock's porosity. Typical value for the rock at the testbed is estimated to be $\phi$=5%.
- $C_t = 10^{-9}$ 1/Pa is the total compressibility including the fluid's and pore space's compressibility.
- $\mu$ = 0.8 cP is water's dynamic viscosity at 30 MPa and 30°C.

Plugging in these parameters, we obtain $C_L$ = 0.006 mm/s$^{0.5}$. The leakoff rate per unit fracture area is $2C_L/t^{0.5}$, where $t$ is the time of the fracture area has been pressurized. After one hour of pressurization, the total leakoff rate per m$^2$ of fracture area would be 12 ml/min. A fracture area of 33 m$^2$ would consume the entire injection rate of 400 ml/min. In other words, it will take hours of injection to even

saturate such a surface area under this hypothetical condition. The 2-hour fluid arrival time is therefore consistent with a rough estimate of the surface area of the hydraulic fracture, which is tens of $m^2$.

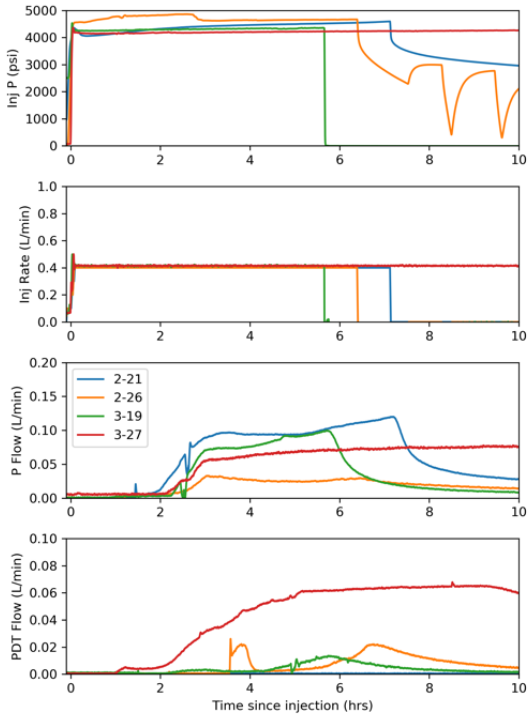


**Figure 6 Results from the four selected "largely independent" injection tests. The axis is adjusted to that the time when injection was started in each test corresponds to the origin.**

### 4.2 Leakoff-dominated fracture propagation

There exists an analytical solution for hydraulic fracture propagation in the leakoff-dominated domain. Here we reiterate the logic behind this equation and proves that it is applicable to the problem studied here although it does not involve propagation of a fracture.

Consider binary states for any point on a fracture: "open" means the two opposing walls are jacked open by pressurized fluid whereas "closed" means the pressure is lower than the "closure stress $S_{\text{closure}}$" and the two opposing walls are in contact. Owing to the "cubic law", the transmissibility of an open fracture is much greater than that for closed fracture, so frictional pressure loss along an open fracture is very low. For the open segment, the fluid pressure only needs to be slightly higher than the closure stress and therefore is approximately constant.

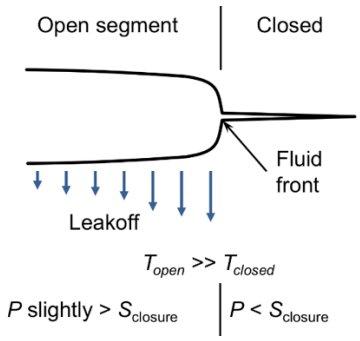


**Figure 7 Conceptual aperture, pressure, and leakoff distribution: differences between open fracture and closed fracture**

For a given fracture area under a constant fluid pressure, the leakoff rate decreases over time as the surrounding rock matrix gets pressurized. Under a constant injection rate, the open area needs to increase, that is, the fracture front or the fluid front needs to propagate, to accommodate the injection. In other words, the open fracture (and the associated fluid front) propagates in a rate that the total leakoff and the fracture volume increase happen to balance the injection rate.

$$L(t) = \frac{qt^{0.5}}{\pi W_f C_L}$$

where $L(t)$ is the total fracture length after injection at a constant rate $q$ for time $t$. Although this equation was originally developed for a propagating fracture (the "closed" part would be intact rock instead of fracture walls in contact), as opposed to the progressive opening of an existing fracture, it applies to both scenarios because rock toughness is ignored anyway. To make $L$(2 hours) = 10 m, which is the approximate distance between the injection and production wells, we need to have $W_f$ = 3 m. In other words, the equivalent total flow channel area between the two wells on the hydraulic fracture is approximately 30 m$^2$.

## 5. ESTIMATING THERMAL PERFORMANCE

With the inferred width ($W_f$) of flow channels in the hydraulic fracture, we further model the long-term circulation test and analyze the thermal responses in the fracture network. We developed a 3D thermal model which includes the fracture network as well as the rock formation surrounding the hydraulic fracture and the OT-P Connector. The two fractures are represented by two thin layers 0.004 m in thickness (Fig. 8(a)). The initial 3D temperature field in the model is obtained from a 2D model by White et al. (2018), which considered the effect of ambient geothermal gradient, hydrological state and historical miming operations (excavation, flooding, dewatering, and mine closure). Fig. 8 (b) shows the flow channel we included in the hydraulic fracture. The aperture within the flow channel is 0.6 mm, and that out of the flow channel is 0.01 mm. The aperture in the OT-P Connector is 1.0 mm.

Fig. 9 shows the injection and outflow rates at different wells (PB, PI, E1-PDT) during the long-term circulation test. The injection rate remained at almost at 400 ml/min except several shut-in periods. However, the outflow rates varied drastically during the test. To appropriately model the flow field in the fracture network, we use step functions to approximate the outflow rate changes in the thermal modeling. Note that we include sink to account for water leakage to natural fractures that are not explicitly included in the model. In the thermal modeling, the sink was used as a pressure boundary. Fig. 8 also shows the injection temperature during the long-term circulation test. Also note started to inject chilled water on May 8 with the injection temperature reduced from 28 °C to 11.5 °C. The parameters for rock and fluid properties used in the thermal modeling are listed in Table 1.

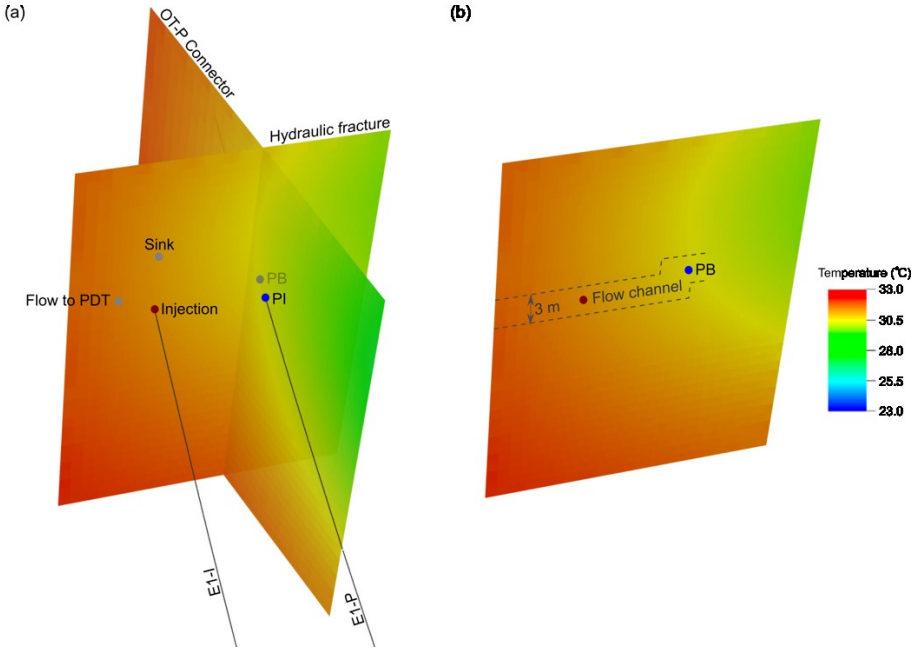


**Figure 8: Initial temperature distribution and flow channel in the thermal model. (a) Initial temperature distribution in the hydraulic fracture and OT-P Connector. (b) A flow channel in the hydraulic fracture.**

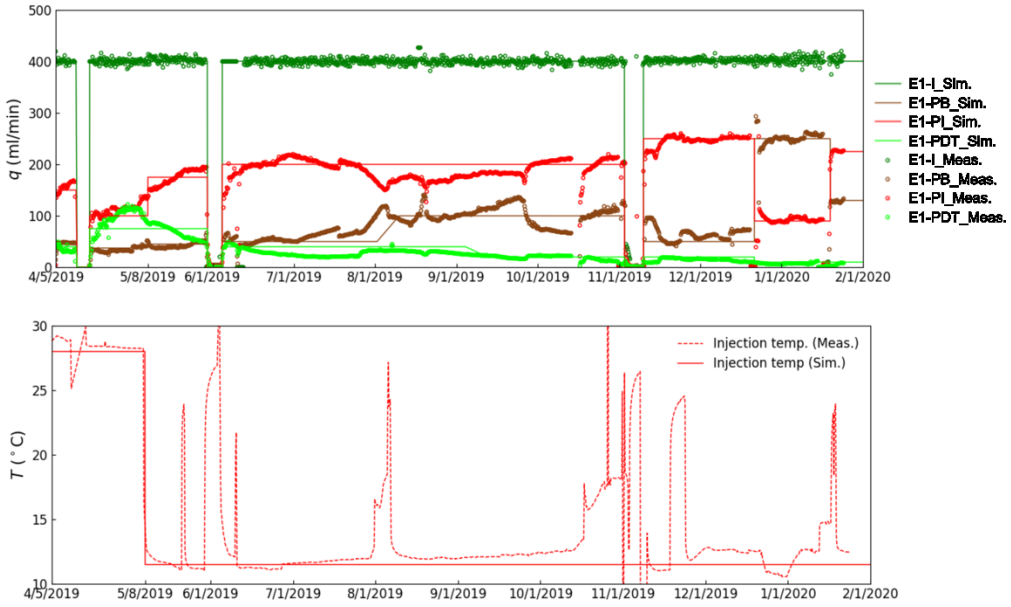


**Figure 9: Injection/outflow rates and injection temperature. (a) Measured injection rate and outflow rates at E1-PB, E1-PI and E1-PDT. (b) Injection temperature. The solid lines are field measurements and the dash lines are fitted step functions used in the thermal simulations.**

**Table 1: Rock and water parameters used for thermal modeling.**

| Parameter | Value | Parameter | Value |
|---|---|---|---|
| Porosity of rock | 0.003 | Permeability of rock ($m^2$) | $2 \times 10^{-18}$ |
| Solid density of rock ($kg/m^3$) | 2500 | Specific heat capacity of rock (J/kg/K) | 790 |
| Specific heat capacity of water (J/kg/K) | 4460 | Water viscosity (Pa·s) | 0.001 |
| Water compressibility ($Pa^{-1}$) | $2 \times 10^{-10}$ | Thermal conductivity of rock (W/m/K) | 5 |

The thermal modeling started on April 5, 2019 and continued for 480 days. Fig. 10 compares the temperature responses at E1-PB with different thermal conductivities. The thermal breakthrough occurs at approximately 24 days after chilled water injection on May 8, 2019. With a larger thermal conductivity, the heat exchange between the chilled water in the hydraulic fracture and the rock formation is more remarkable, and therefore the temperature decrease at E1-PB is smaller. The temperature increase at around 210 days is due to the shut-in operation and the significant decrease of the outflow rate at E1-PB (Fig. 9).

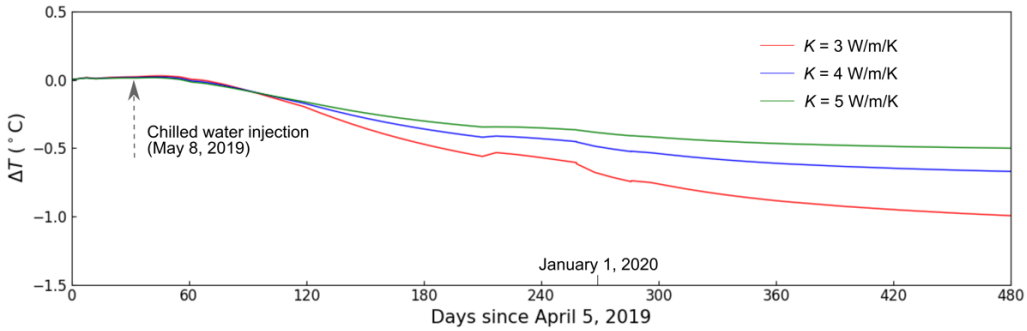


**Figure 10: Comparison of thermal responses at E1-PB with different thermal conductivity.**

## 6. CONCLUSIONS

In this paper, we present our effort to quantify the total flow channel area engaged in the long-term circulation test at the Collab Experiment 1 testbed. The fracture network carrying the flow includes a hydraulic fracture and a major natural fracture. Because the intersection between the two main fracture is near the production well, the arrival time of fluid to the production well is mainly influenced by flow on the hydraulic fracture. In four short-term injection tests, fluid arrived at the production well after 2 hours of injection, forming a very consistent pattern. We argue that during this process, the fluid front propagates in the leakoff-dominated regime. A close-form solution allows to estimate the total flow channel width to be approximately 3 m, which is one order of magnitude smaller than the overall dimension of the fracture. A thermal modeling using this result shows that it still take several hundred days for a significant thermal breakthrough to be observed. For the circulation test performed so far, the temperature change in PB is obscured by Joule-Thomson effect, which increases water temperature by several degrees. Nevertheless, the estimated of the total flow channel width could be used for understanding the testbed itself and many other tests performed there.

## ACKNOWLEDGMENTS

This manuscript has been authored by Lawrence Livermore National Security, LLC under Contract No. DE-AC52-07NA27344 with the US. Department of Energy. This research was also supported by the U.S. Department of Energy, Geothermal Technologies Office (GTO). The United States Government retains, and the publisher, by accepting the article for publication, acknowledges that the United States Government retains a non-exclusive, paid-up, irrevocable, world-wide license to publish or reproduce the published form of this manuscript, or allow others to do so, for United States Government purposes. We thank the drillers of Agapito Associates, Inc., for their skill and dedicated efforts to create our test bed boreholes. The research supporting this work took place in whole or in part at the Sanford Underground Research Facility in Lead, South Dakota. The assistance of the Sanford Underground Research Facility and its personnel in providing physical access and general logistical and technical support is gratefully acknowledged.

Support from the EGS Collab Team is gratefully acknowledged. EGS Collab Team includes J. Ajo-Franklin, T. Baumgartner, K. Beckers, D. Blankenship, A. Bonneville, L. Boyd, S. Brown, J.A. Burghardt, C. Chai, Y. Chen, B. Chi, K. Condon, P.J. Cook, D. Crandall, P.F. Dobson, T. Doe, C.A. Doughty, D. Elsworth, J. Feldman, Z. Feng, A. Foris, L.P. Frash, Z. Frone, P. Fu, K. Gao, A. Ghassemi, Y. Guglielmi, B. Haimson, A. Hawkins, J. Heise, C. Hopp, M. Horn, R.N. Horne, J. Horner, M. Hu, H. Huang, L. Huang, K.J. Im, M. Ingraham, E. Jafarov, R.S. Jayne, S.E. Johnson, T.C. Johnson, B. Johnston, K. Kim, D.K. King, T. Kneafsey, H. Knox, J. Knox, D. Kumar, M. Lee, K. Li, Z. Li, M. Maceira, P. Mackey, N. Makedonska, E. Mattson, M.W. McClure, J. McLennan, C. Medler, R.J. Mellors, E. Metcalfe, J. Moore, C.E. Morency, J.P. Morris, T. Myers, S. Nakagawa, G. Neupane, G. Newman, A. Nieto, C.M. Oldenburg, T. Paronish, R. Pawar, P. Petrov, B. Pietzyk, R. Podgorney, Y. Polsky, J. Pope, S. Porse, J.C. Primo, C. Reimers, B.Q. Roberts, M. Robertson, W. Roggenthen, J. Rutqvist, D. Rynders, M. Schoenball, P. Schwering, V. Sesetty, C.S. Sherman, A. Singh, M.M. Smith, H. Sone, E.L. Sonnenthal, F.A. Soom, P. Sprinkle, C.E. Strickland, J. Su, D. Templeton, J.N. Thomle, V.R. Tribaldos, C. Ulrich, N. Uzunlar, A. Vachaparampil, C.A. Valladao, W. Vandermeer, G. Vandine, D. Vardiman, V.R. Vermeul, J.L. Wagoner, H.F. Wang, J. Weers, N. Welch, J. White, M.D. White, P. Winterfeld, T. Wood, S. Workman, H. Wu, Y.S. Wu, E.C. Yildirim, Y. Zhang, Y.Q. Zhang, Q. Zhou, M.D. Zoback

## REFERENCES

Fu, P., M. White, J. Morris, T. Kneafsey, and E.C. Team (2018), Predicting Hydraulic Fracture Trajectory Under the Influence of a Mine Drift in EGS Collab Experiment I, in *PROCEEDINGS*, 43rd Workshop on Geothermal Reservoir Engineering, Stanford University, Stanford, CA (2018).

Frash, L. et al.: GS Collab Experiment 1 Site Geomechanical and Hydrological Properties by Triaxial Direct Shear. in *PROCEEDINGS*, 44th Workshop on Geothermal Reservoir Engineering, Stanford University, Stanford, CA (2020).

Guo, B. et al.: Thermal drawdown-induced flow channeling in a single fracture in EGS. Geothermics, 61:46-62.

Hawkins, A.J., Becker, M.W., Tester, J.W.: Inert and adsorptive tracer tests for field measurement of flow-wetted surface area, *Water Resources Research*, **54**, (2018), 5341-5358.

Kneafsey, T.J. et al: The EGS Collab Project: Learnings from Experiment 1, in *PROCEEDINGS*, 45th Workshop on Geothermal Reservoir Engineering, Stanford University, Stanford, CA (2020).

Ghanashyam, N. et al: Results of Multiple Tracer Injections Into Fractures in the EGS Collab Testbed-1, , in *PROCEEDINGS*, 45th Workshop on Geothermal Reservoir Engineering, Stanford University, Stanford, CA (2020).

Oldenburg, C.M., P.F. Dobson, Y. Wu, P.J. Cook, T.J. Kneafsey, S. Nakagawa, C. Ulrich, D.L. Siler, Y. Guglielmi, J. Ajo-Franklin, J. Rutqvist, T.M. Daley, J.T. Birkholzer, H. Wang, N.E. Lord, B.C. Haimson, H. Sone, P. Vigilante, W.M. Roggenthen, T.W. Doe, M.Y. Lee, M. Ingraham, H. Huang, E.D. Mattson, J. Zhou, T.J. Johnson, M.D. Zoback, J.P. Morris, J.A. White, P.A. Johnson, D. DD. Coblentz, and J. Heise.: *Intermediate-Scale Hydraulic Fracturing in a Deep Mine, kISMET Project Summary 2016*, LBNL-1006444, Lawrence Berkeley National Laboratory, Berkeley, CA (2016). DOI: 10.2172/1338937.

Tsang, Y.W., Tsang, C., 1987. Channel model of flow through fractured media.Water Resour. Res. 23 (3), 467–479.

White, M.D., Fu, P.C., Ghassemi, A., Huang, H., Rutqvist, J., Johnston, B., EGS Collab: Numerical simulation applications in the design of EGS Collab Experiment 1, 43rd Stanford Geothermal Workshop, Stanford University, Stanford, CA (2018).